This is the pre-print version of an article finally published as:
Fernández C, González-Rubio G, Langer J, Tardajos G. Liz-Marzán L, Giraldo R, Guerrero-Martínez A (2016) Nucleation of amyloid oligomers by RepA-WH1-prionoid-functionalized gold nanorods. Angew. Chem. Int. Ed. 55: 11237-11241. Doi: 10.1002/anie.201604970

Nucleation of Amyloid Oligomers by RepA-WH1 Prionoid- Functionalized Gold Nanorods

Cristina Fernández+, **Guillermo González-Rubio**+, **Judith Langer**, **Gloria Tardajos**, **Luis M. Liz-Marzán**, **Rafael Giraldo***, and **Andrés Guerrero-Martínez***

Dr. C. Fernández [+], Prof. R. Giraldo [*], Department of Cellular and Molecular Biology Centro de Investigaciones Biológicas—CSIC 28040 Madrid (Spain). E-mail: rgiraldo@cib.csic.es

G. González-Rubio [+], Prof. G. Tardajos, Dr. A. Guerrero-Martínez [*], Departamento de Química Física I, Universidad Complutense de Madrid, Avda. Complutense s/n, 28040 Madrid (Spain). E-mail: aguerrero@quim.ucm.es

G. González-Rubio [+], Dr. J. Langer, Prof. L. M. Liz-Marzán, BioNanoPlasmonics Laboratory, CIC biomaGUNE, Donostia—20009 San Sebastián (Spain)

Prof. L. M. Liz-Marzán, Ikerbasque, Basque Foundation for Science, 48013 Bilbao (Spain), and Biomedical Research Networking Center in Bioengineering, Biomaterials, and Nanomedicine, CIBER-BBN (Spain)

[+] These authors contributed equally to this work.

Abstract

Understanding protein amyloidogenesis is an important topic in protein science, fueled by the role of amyloid aggregates, especially oligomers, in the etiology of a number of devastating human degenerative diseases. However, the mechanisms that determine the formation of amyloid oligomers remain elusive due to the high complexity of the amyloidogenesis process. For instance, gold nanoparticles promote or inhibit amyloid fibrillation. We have functionalized gold nanorods with a metal-chelating group to selectively immobilize soluble RepA-WH1, a model synthetic bacterial prionoid, using a hexa-histidine tag (H6). H6-RepA-WH1 undergoes stable amyloid oligomerization in the presence of catalytic concentrations of anisotropic nanoparticles. Then, in a physically separated event, such oligomers promote the growth of amyloid fibers of untagged RepA-WH1. SERS spectral changes of H6-RepA-WH1 on spherical citrate-AuNP substrates provide evidence for structural modifications in the protein, which are compatible with a gradual increase in β-sheet structure, as expected in amyloid oligomerization.

Protein amyloidoses such as Alzheimer's, Parkinson's, and prion-related diseases are the focus of intense research due to their deep impact on human health.[1] Amyloidogenesis is a nearly universal process for the conformational conversion between the native and aggregated states of proteins, with implications for essential physiological processes.[2] Among the distinct association states that any protein transits from the native and soluble states to the fully aggregated amyloid condition, that is, small oligomeric assemblies, large oligomers, and fibers, the first are the most toxic and thus disease-relevant species.[3]

Among the experimental techniques used to characterize amyloidogenesis *in vitro*, spectroscopy occupies a central position. Namely, UV/Vis absorption spectroscopy has been used to study the binding of the amyloidotropic stain Congo red, often detected as green birefringence under a polarized light microscope.[4] Fluorescence spectroscopy is also used to investigate amyloidogenesis through the binding of extrinsic fluorophores, which increase and/or shift their fluorescence emission upon intercalation between the b-sheets that constitute the characteristic amyloid cross-β fold.[5] For these techniques, a rather mature fibrillar or prefibrillar form is required to achieve sufficient binding of the probes. These molecules are thus not efficient for the investigation of early amyloidogenic oligomers.[1–3]

Surface-enhanced Raman scattering (SERS) spectroscopy has emerged as a useful technique for sensing amyloid proteins at the surface of plasmonic gold nanoparticles (AuNPs),[6] since the chemical nature and 3D arrangement of the proteins determine a unique and enhanced Raman vibrational fingerprint.[7] Analogously to other organic and inorganic nanomaterials,[8] AuNPs features, such as the size, charge, and shape, can either promote[9] or inhibit[10] the templating ability of amyloids due to metal–protein interactions. Although these investigations focused mainly on the formation of fibrillar and prefibrillar amyloids,[11] the direct observation of AuNP-induced nucleation of amyloid oligo- mers at the early stages of amyloidogenesis by SERS has not been reported.

The synthetic prionoid RepA-WH1, the N-terminal domain of the bacterial plasmid replication protein RepA,[5b] is an attractive model system to explore the nucleation of amyloid oligomers. Similarly to the mammalian prion PrP,[12] and besides the protein-to-protein templating of the amyloid conformation, nucleic acids (dsDNA) and acidic phospholipids promote the amyloidosis of RepA-WH1, both in vitro and in vivo.[13] This protein undergoes a substantial conformational change from soluble stable dimers to metastable aggregation-prone monomers that then assemble into amyloid fibers.[14] RepA-WH1, in particular its hyper-amyloidogenic mutant variant A31V, H6-RepA-WH1(A31V), causes in bacteria a type of amyloidosis that shares many features with mammalian neurodegenerative diseases,[15] while remaining bio-safe for humans.

Herein, we describe the formation of amyloid oligomers with different molecular weights, induced by gold nanorods (AuNRs) functionalized with the H6-RepA-WH1(A31V) prionoid. Furthermore, we used such oligomers to trigger the growth of amyloid fibril superstructures (**Scheme 1**). AuNRs were chosen over the more commonly-used spherical AuNPs due to their higher sensitivity to small changes in their dielectric environments, combined with a high reactivity, which facilitates molecular functionalization.[16]

AuNRs were first functionalized with thiolated polyethylene glycol to provide colloidal stability in buffer media and co-functionalized with lipoic acid (see the Supporting Information).[17] Immobilization of H6-RepA-WH1(A31V) was achieved after the specific modification of the AuNR surface with the lipoic amide-nitrilotriacetic-CoII complex

(ANTACo).[18] This chemical functionality specifically reacts with the H6 hexa-histidine chain (**Scheme 1**), avoiding undesired coupling to any of the multiple free amine groups in the protein. The ANTACo-functionalized AuNRs were incubated at $1:10^5$ and 1:50 AuNR:H6-RepA-WH1(A31V) molar ratios, with protein concentrations of 20 and 0.1 μM, respectively. This protein forms a stable dimer in solution under a broad range of conditions (Scheme 1).[13a, 14, 19] However, the observed 5 nm red shift of the AuNRs longitudinal localized surface plasmon resonance (LSPR) at both molar ratios, indicates the absence of AuNR self-assembly in solution (**Figure 1A**, see the Supporting Information).[20] This might be expected from the presence of two oppositely anchored H6 groups on the H6-RepA-WH1(A31V) dimers (**Scheme 1**). These results point to the immobilization of the protein in its pre-amyloidogenic monomeric state on the metal surface, which is a necessary intermediate step in the ligand-promoted assembly of the protein as amyloids.[13a, 14, 19] The same incubation experiments were performed with spherical AuNPs of comparable (ca. $2x10^3$ nm^2) and larger (ca. $1.1x10^4$ nm^2) surface areas. Non-significant changes of the LSPRs were observed (see the Supporting Information), showing the convenience of using AuNRs for monitoring the protein functionalization process.

After 24h, the mixture at the $1:10^5$ AuNR:H6-RepA-WH1(A31V) molar ratio was centrifuged to separate the precipitate formed during the incubation, containing AuNRs and protein aggregates, from the soluble H6-RepA-WH1(A31V). No precipitation of the protein was observed under the same conditions in the absence of AuNRs. Finally, the pellet was redispersed in buffer. To verify the coating of AuNRs by H6-RepA-WH1(A31V), immunoelectron microscopy (iEM) was carried out using a polyclonal anti-WH1 antibody (see the Supporting Information).[13c] Secondary antibodies conjugated to the spherical AuNPs (10 nm Ø) were consistently found around the AuNRs (7:1), although some unattached protein aggregated in the background (1:1) (**Figure 1B**, see the Supporting Information). When the mixture was stored for long periods of time (up to 4 weeks) at 4 ^oC, several oligomeric species of H6-RepA-WH1(A31V) were identified by means of denaturing gel electrophoresis (SDS-PAGE). The presence of a ladder with progressively higher molecular weights (**Figure 1C**) reveals protein complexes that persisted under the extreme denaturing conditions (detergent plus boiling) of the electrophoresis (see the Supporting Information), consistent with the high stability of amyloids.[15b] This result suggests a dynamic process in which, over time, amorphous pre-amyloidogenic aggregates are converted into amyloid oligomers.

Immunoblotting with B3h7, an antibody specific for an oligomeric and pre-amyloidogenic form of H6-RepA-WH1(A31V),[13c] yielded more intense binding to a protein sample stored for 22 days than to the native protein, even at the highest dilution of the antigen (**Figure 2A**, see the Supporting Information). However, the conformation-unspecific anti-WH1 antibody recognized both samples equally well at their full range of concentrations. This experiment clearly demonstrates that the oligomers nucleated by AuNRs are amyloidogenic in nature. When such oligomers were used as seeds (that is, polymerization-nucleating agents) in incubations with soluble and untagged RepA-WH1(A31V), characteristic amyloid straight and unbranched fibers with 24.6 +/- 0.7 nm cross-sectional thickness were grown, as observed by TEM analysis (**Figure 2 B**).[13a, 14] Analogous experiments showed that occasional and less-structured fibers were formed in the presence of non-functionalized AuNRs (see the Supporting Information), which highlight the importance of the prionoid functionalization in the fibrillation.

Additionally, we used SERS spectroscopy to explore the transition from α-helix into β-sheet conformation (a signature for amyloidogenesis) in the oligomers obtained after the incubation of H6-RepA-WH1(A31V) with AuNRs. The SERS spectra of the native proteins and their oligomers were obtained using citrate-coated AuNPs (60 nm Ø) (**Figure 3A**, see the Supporting Information), because of their high performance and plasmonic efficiency in SERS when aggregated on a substrate.[21] SERS spectra were collected using 785 nm laser light as the excitation source, at low intensity (1.4 $\mu W \cdot cm^{-2}$) to avoid damaging the samples. Under such conditions, the typical band broadening characteristic of the Raman spectra of proteins was observed.[22] SERS spectra were obtained for the native protein and at the initial (1 day) and final (22 days) stages of oligomerization. Incubation of H6-RepA-WH1(A31V) with AuNRs induced variations in the full range of the SERS spectrum, as compared to the native protein (**Figure 3**, see **Table 1** in the Supporting Information). Non-significant changes in the positions of the Raman signals were observed at different stages of the oligomerization, but line broadening resulted as the molecular weight of the oligomers increased.

Information about modifications in the tertiary structure of the oligomers can be extracted from changes at the low wavenumber region of the SERS spectra. This is the case for the two new intense bands at 1357 and 1399 cm^{-1}, associated with the C-C stretching, C-H deformation, and backbone vibrations (**Figure 3A**). Although it is not possible to directly relate these bands to the amyloid conformation, their presence in the oligomers, but not in the native protein, clearly indicates a rearrangement in H6-RepA-WH1(A31V) when amyloidogenesis occurs.

Regarding the amyloid structure, the interactions between the backbone amide and carbonyl groups through hydrogen bonding, such as those responsible for the β-sheet structure in the amyloid fold, present nine vibrational modes, of which amides III and I are highly sensitive to changes in the secondary structure. The former ranges from 1220 and 1300 cm^{-1} (**Figure 3B**), while the latter occurs between 1600 and 1700 cm^{-1} (**Figure 3C**).[5, 17] The amide III region of the native conformation is dominated by bands at 1222 and 1265 cm^{-1}, which are linked to aromatic residues and a random structure, whereas amide I does not show any Raman signal. On the other hand, we can observe two new bands at 1242 and 1290 cm^{-1}, attributed to the formation of β-sheets and the deformation of α-helices, respectively.[22] The latter might reflect the formation of a β-solenoid, a helical arrangement of β-strands common to some amyloid proteins.[23] This observation is also supported by two new bands at 1648 and 1670 cm^{-1} in the amide I region, which correspond to the α-helix and β-sheet secondary structures, respectively.

In summary, we have provided evidence for the feasibility of using prionoid-functionalized AuNRs as nucleating agents for controlled protein amyloidosis *in vitro*. The proposed mechanism of AuNR-mediated amyloid nucleation is based on a conformational change from the dimer protein precursor to the immobilized pre-amyloidogenic monomer at the nanoparticle surface, which promotes efficient amyloid oligomerization and fibrillation. Our results show the potential of using prionoid-functionalized AuNRs to understand amyloid oligomer formation and the disadvantage of such strategy to achieve early detection of amyloid diseases *in vitro* and *in vivo*, considering that the presence of the AuNPs can itself be amyloidogenic. We are currently exploring the possibility of using this system as a controlled model to understand protein amyloidogenesis *in vivo*.

Acknowledgements

Research at the R.G. laboratory was supported by MINECO grants CSD2009-00088, BIO2012-30852 and BIO2015-68730- R. Research at the A.G-M. and L.M.L-M. laboratories was supported by MINECO (MAT2014-59678-R and MAT2013-46101-R), Madrid Regional Government (S2013/MIT-2807) and the "*I Convocatoria de Ayudas Fundación BBVA a Investigadores, Innovadores y Creadores Culturales*" (14_CBB_147) grants. A.G-M. and G.G-R. acknowledge, respectively, receipt of "*Ramón y Cajal*" and FPI Fellowships from the Spanish MINECO.

Keywords: amyloidosis · gold nanorods · oligomers · prions · SERS

References

[1] P. Westermark, M. D. Benson, J. N. Buxbaum, A. S. Cohen, B. Frangione, S. Ikeda, C. K. Masters, G. Merlini, M. J. Saraiva, J. D. Sipe, Amyloid 2002, 9, 197 – 200.

[2] T. P. J. Knowles, M. Vendruscolo, C. M. Dobson, Nat. Rev. Mol. Cell Biol. 2014, 15, 384 – 396.

[3] a) T. Eichner, S. E. Radford, Mol. Cell 2011, 43, 8 – 18 ; b) A. K. Schütz, A. Soragni, S. Hornemann, A. Aguzzi, M. Ernst, A. Bçckmann, B. H. Meier, Angew. Chem. Int. Ed. 2011, 50, 5956 – 5960 ; Angew. Chem. 2011, 123, 6078 – 6082.

[4] C. Wu, Z. Wang, H. Lei, Y. Duan, M. T. Bowers, J. E. Shea, J. Mol. Biol. 2008, 384, 718 – 729.

[5] a) N.P.R. Nilsson, FEBS Lett. 2009, 583, 2593–2599; b) R. Giraldo, J. M. Andreu, R. Díaz-Orejas, EMBO J. 1998, 17, 4511 – 4526.

[6] a) I. Choi, Y. S. Huh, D. Erickson, Microfluid. Nanofluid. 2012, 12, 663 – 669 ; b) R. A. lvarez-Puebla, A. Agarwal, P. Manna, B. P. Khanal, P. Aldeanueva-Potel, E. Carbó-Argibay, N. Pazos- PØrez, L. Vigderman, E. R. Zubarev, N. A. Kotov, L. M. Liz- Marzµn, Proc. Natl. Acad. Sci. USA 2011, 108, 8157 – 8161; c) L. Guerrini, R. Arenal, M. Benedetta, F. Chiti, R. Pini, P. Matteini, R. A. Alvarez-Puebla, ACS Appl. Mater. Interfaces 2015, 7, 9420 – 9428 ; d) I.-H. Chou, M. Benford, H. T. Beier, G. L. CotØ, Nano Lett. 2008, 8, 1729 – 1735.

[7] G. J. Takashi, T. J. Miura in Proteins: Structure, Function, and Engineering (Ed.: B. B. Biswas, S. Roy), Springer Science, New York, 1995, pp. 55 – 99.

[8] a) C. Cabaleiro-Lago,F.Quinlan-Pluck,I.Lynch,K.A.Dawson, S. Linse, ACS Chem. Neurosci. 2010, 1, 279–287; b) A.-M. Yousefi, Y. Zhoy, A. Querejeta-Fernández, K. Sun, N. A. Kotov, J. Phys. Chem. Lett. 2012, 3, 3249 – 3256 ; c) Z. S. Al-Garawi, J. R. Thorpe, L. C. Serpell, Angew. Chem. Int. Ed. 2015, 54, 13327 – 13331; Angew. Chem. 2015, 127, 13525 – 13529.

[9] Y.-H. Liao, Y.-J. Chang, Y. Yoshiike, Y.-C. Chang, Y.-R. Chen, Small 2012, 8, 3631 – 3639.

[10] D. A. Yanina, J. A. Fauerbach, J. V. Pellegrotti, T. M. Jovin, E. A. Jares-Erijman, F. D. Stefani, Nano Lett. 2013, 13, 6156 – 6163.

[11] Y. Kim, J.-H. Part, H. Lee, J.-M. Nam, Sci. Rep. 2016, 6, 19548.

[12] J. L. Silva, L. M. Lima, D. Foguel, Y. Cordeiro, Trends Biochem. Sci. 2008, 33, 132 – 140.

[13] a) R. Giraldo, Proc. Natl. Acad. Sci. USA 2007, 104, 17388 – 17393; b) F. Gasset-Rosa, M. J. Maté, C. Dávila-Fajardo, J. Bravo, R. Giraldo, Nucleic Acids Res. 2008, 36, 2249–2256; c) M. Moreno-del Álamo, S. Moreno-Díaz de la Espina, M. E. Fernández-Tresguerres, R. Giraldo, Sci. Rep. 2015, 5, 14669–14672; d) C. Fernández, R. Nuñez-Ramírez, M. Jiménez, G. Rivas, R. Giraldo, Sci. Rep. 2016, 6, 23144.

[14] E. Torreira, M. Moreno-del Álamo, M. E. Fuentes-Perez, C. Fernández, J. Martín-Benito, F. Moreno-Herrero, R. Giraldo, O. Llorca, Structure 2015, 23, 183 – 189.
[15] a) M. E. Fernández-Tresguerres, S. Moreno-Díaz de la Espina, F. Gasset-Rosa, R. Giraldo, Mol. Microbiol. 2010, 77, 1456– 1469; b) F. Gasset-Rosa, A. S. Coquel, M. Moreno-del Álamo, P. Chen, X. Song, A. M. Serrano, M. E. Fernández-Tresguerres, S. Moreno-Díaz de la Espina, A. B. Lindner, R. Giraldo, Mol. Microbiol. 2014, 91, 1070 – 1087.
[16] C. J. Murphy, T. K. Sau, A. M. Gole, C. J. Orendorff, J. Gao, L. Gou, S. E. Hunyadi, T. Li, J. Phys. Chem. B 2005, 109, 13857 – 13870.
[17] E. Oh, K. Susumu, A. J. Mäkinen, J. R. Deschamps, A. L. Huston, I. L. Medintz, J. Phys. Chem. C 2013, 117, 18947 – 18956.
[18] J. M. Abad, S. F. L. Mertens, M. Pita, V. M. Fernández, D. J. Schiffrin, J. Am. Chem. Soc. 2005, 127, 5689 – 5694.
[19] R. Giraldo, C. Fernández-Tornero, P. R. Evans, R. Díaz-Orejas, A. Romero, Nat. Struct. Biol. 2003, 10, 565 – 571.
[20] a) A. Guerrero-Martínez, M. Grzelczak, L. M. Liz-Marzán, ACS Nano 2012, 6, 3655 – 3662; b) K. K. Caswell, J. N. Wilson, U. H. F. Bunz, C. J. Murphy, J. Am. Chem. Soc. 2003, 125, 13914 – 13915.
[21] a) C. Costas, V. López-Puente, G. Bodelón, C. González-Bello, J. Pérez-Juste, I. Pastoriza-Santos, L. M. Liz-Marzán, ACS Nano 2015, 9, 5567 – 5576 ; b) C. Hamon, M. S. Novikov, L. Scarabelli, D. M. Solís, T. Altantzis, S. Bals, J. M. Taboada, F. Obelleiro, L. Liz-Marzán, M. Luis, ACS Photonics 2015, 2, 1482 – 1488.
[22] D. Nemecek, J. Stepankek, G. J. Thomas, Current Protocols in Protein Science. 2013, 71, 17.8:17.8.1–17.8.52.
[23] A. V. Kajava, U. Baxa, A. C. Steven, FASEB J. 2010, 24, 1311 – 1319.

FIGURES

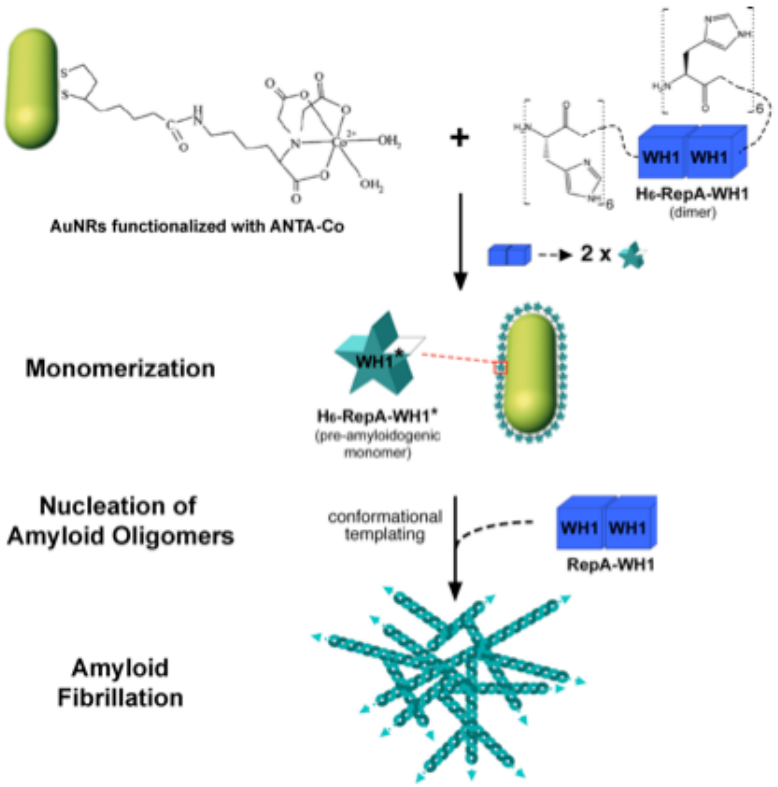

Scheme 1. Outline of the nucleation of RepA-WH1 amyloidogenesis by prionoid-functionalized AuNRs. Pre-amyloidogenic RepA-WH1 monomers (stars) are generated on the AuNR surface from the initial RepA-WH1 dimers (cubes).[15a] Such functionalization induces the formation of oligomers that can be used as seeds for amyloid fibrillation.

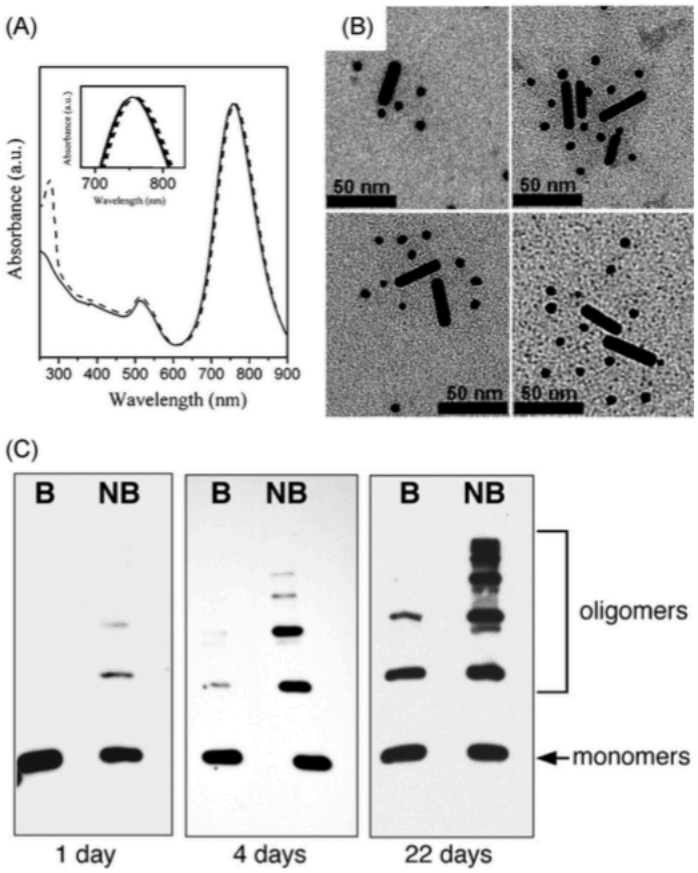

Figure 1. **A**) UV/Vis spectra of AuNRs in the absence (solid line) and presence (dash line) of H6-RepA-WH1(A31V) after 24 h of incubation (1:10^5 AuNR:H6-RepA-WH1(A31V) molar ratio with 20 μM of protein). The inset shows a detail of the 5 nm red shift observed under incubation. **B**) iEM of AuNRs incubated with H6-RepA-WH1(A31V) in (A) and the primary antibody (anti-WH1), attached to secondary Au-conjugated antibody clusters. **C**) SDS-PAGE plus Western-blotting (anti-WH1) of the AuNRs in (B). B tracks: boiled samples; NB tracks: not boiled. The protein undergoes oligomerization on the particles, indicating the transition to a pre-amyloidogenic state.

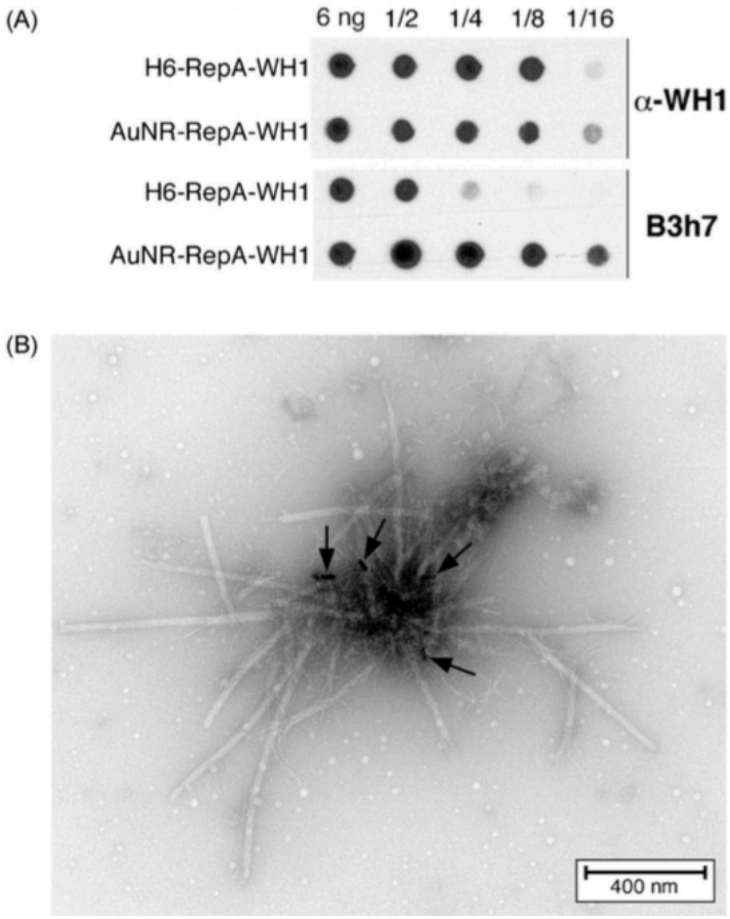

Figure 2. **A**) The dot-blot assay with B3h7, an antibody specific for amyloidogenic RepA-WH1 oligomers,[13c] reveals that the H6-RepA-WH1(A31V) protein assemblies around the AuNRs (even rows) are amyloids, whereas the soluble protein molecules (odd rows) are not. **B**) Mature AuNRs incubated with H6-RepA-WH1(A31V) (indicated by arrows) nucleate the growth of RepA-WH1(A31V) amyloid fibers.

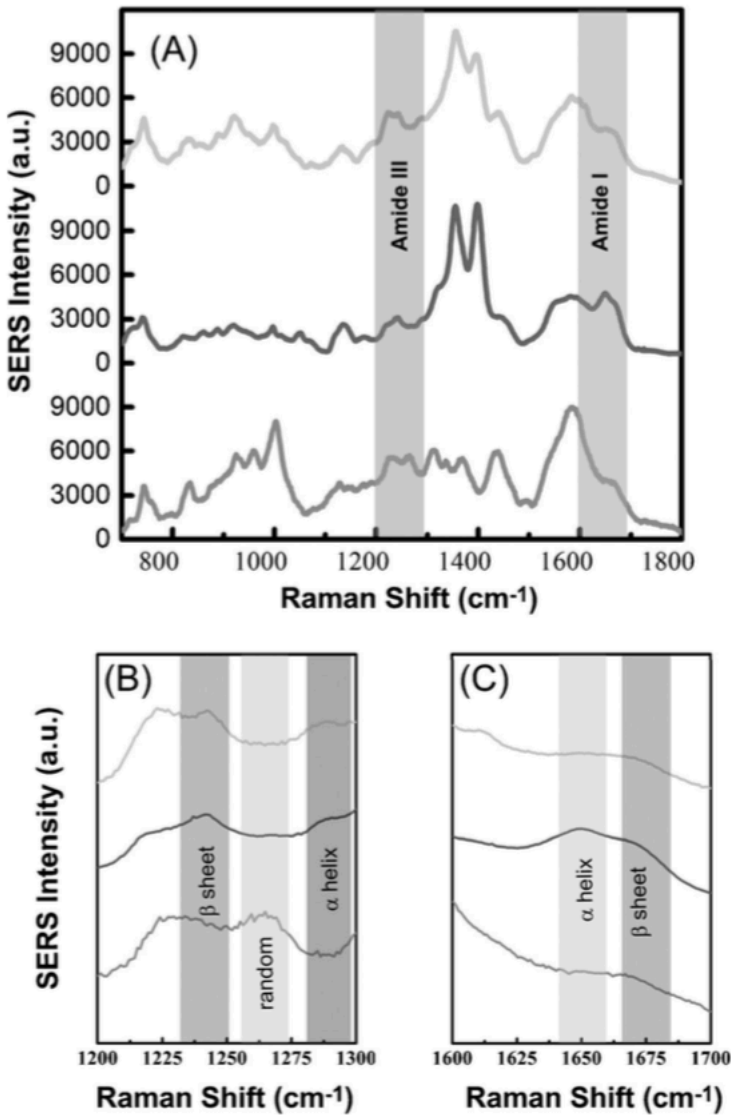

Figure 3. **A**) SERS spectra of the native protein dimers (bottom) and amyloid oligomers of low (middle) and high molecular weights (top), excited at 785 nm. **B,C**) Magnification of the amide III and I regions, respectively.

Supporting Information

Nucleation of RepA-WH1 Amyloid Oligomers by Prionoid Functionalized-Gold Nanorods

Cristina Fernández,[†,‡] Guillermo González-Rubio, [#,||,‡] Judith Langer,[||] Gloria Tardajos,[#] Luis M. Liz-Marzán,[||,⊥,$] Rafael Giraldo,[*,†] and Andrés Guerrero-Martínez[*,#]

[†]Department of Cellular and Molecular Biology, Centro de Investigaciones Biológicas – CSIC, Madrid E28040, Spain
[#]Departamento de Química Física I, Universidad Complutense de Madrid, , Madrid E28040, Spain
[||]BioNanoPlasmonics Laboratory, CIC biomaGUNE, Donostia - San Sebastián E20009, Spain
[⊥]Ikerbasque, Basque Foundation for Science, Bilbao E48013, Spain
[$]Biomedical Research Networking Center in Bioengineering, Biomaterials, and Nanomedicine, CIBER-BBN, Spain
[‡] These authors contributed equally to this work

Materials

All the starting materials were obtained from commercial suppliers and used without further purification: Hexadecyltrimethylammonium bromide (CTAB, ≥99%), Hexadecyltrimethylammonium chloride (CTAC, 25% w/w in water), 5-bromosalicylic acid (technical grade, 90%), hydrogen tetrachloroaurate trihydrate ($HAuCl_4 \cdot H_2O$, ≥99.9%), silver nitrate ($AgNO_3$, ≥99.0%), L-ascorbic acid (≥99%), sodium borohydride ($NaBH_4$, 99%), poly(ethylene glycol) methyl ether thiol (PegSH, Mn 6000), (±)-α-Lipoic acid (0≥98.0%), N_α,N_α-Bis(carboxymethyl)-L-lysine hydrate (ANTA, ≥97.0%, TLC**),** cobalt(II) chloride hexahydrate (ACS reagent, 98%), *N*-(3-Dimethylaminopropyl)-*N*′-ethylcarbodiimide hydrochloride (EDC, purum, ≥98.0% (AT)), N-Hydroxysuccinimide (NHS, 98%) were purchased from Aldrich. Nanopure water (resistivity 18.2 MΩ cm at 25 °C) was used in all experiments**.**

Synthesis and characterization of AuNRs

The seeds were prepared by the standard CTAB/$NaBH_4$ procedure: 25 μL of a 0.05 M $HAuCl_4$ solution was added to 4.7 mL of 0.1 M CTAB solution; 300 μL of a freshly prepared 0.01 M $NaBH_4$ solution was then injected under vigorous stirring. Excess borohydride was consumed by keeping the seed solution for 30 min at room temperature prior to use. Gold nanorods were prepared, with some modifications, as previously

described by Murray and co-workers. In a typical synthesis of a 50 mL nanorod solution, 45 mg of 5-bromosalicylic acid was added to 50 mL of 0.05 M CTAB. The solution was mildly stirred for 15 min until complete dissolution, and 480 µL of 0.01 M $AgNO_3$ and 500 µL of 0.05 M $HAuCl_4$ solutions were added to the mixture. After 40 min, 130 µL of 0.1 M ascorbic acid solution was added under vigorous stirring, followed by 80 µL of seed solution. The mixture was left undisturbed at room temperature for at least 4 h. The resulting gold nanorods presented a LSRP with an absorption maximum at 760 nm (Figure S1A). Typically, the mixture was centrifuge (7000 rpm, 30 min) and finally, nanorods were redispersed in 10 mL of 2 mM CTAB solution.

UV/Vis/NIR absorption spectra of the resulting AuNRs were registered using a Cary 5000 UV-Vis-NIR (Figure S1A). All experiments were carried out at 298 K, using quartz cuvettes with optical paths of 0.1 or 1 cm. TEM images of AuNRs were obtained with a JEOL JEM-1400PLUS transmission electron microscope, operating at an acceleration voltage of 120 kV. Carbon-coated 400 square mesh copper grids were used. All samples were centrifuged at least once before blotting on the grid. The resulting CTAB-stabilized AuNSs (CTAB-AuNRs) presented a length and diameter of 53 ± 4 nm and 14± 1 nm, respectively, and an aspect ratio of 3.7 ± 0.5, as determined from TEM images (Figure S1B).

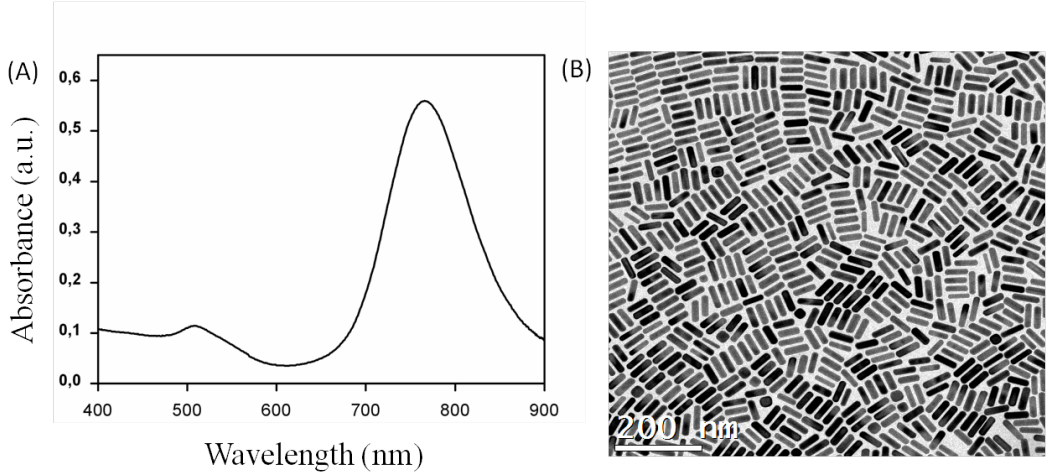

Figure S1. (A) Extinction spectra and (B) representative TEM image of synthesized CTAB-AuNRs in water.

Synthesis and characterization of AuNSs

The seeds were prepared by the standard CTAC/$NaBH_4$ procedure with minor modifications: 50 µL of a 0.05 M $HAuCl_4$ solution was added to 5 mL of 0.1 M CTAC

solution; 200 µL of a freshly prepared 0.02 M $NaBH_4$ (7,6 mg/10 mL) solution was then injected under vigorous stirring. After 3 min the seed was diluted 10 times in CTAC 100 mM.

10nm Spheres: 900 µL of the seed and 40 µL 0.1 M Ascorbic acid were added to 10 mL of 25 mM CTAC solution. Then, 50 µL of a 0.05 M $HAuCl_4$ solution was added under vigorous stirring. The mixture was left undisturbed at room temperature for at least 10 min.

25 nm and 60 nm Spheres: *Step 1:* 200 µL (for the 25 nm spheres) or 50 µL (for the 60 nm) of 10 nm NS suspension, and 25 µL 0.1 M of ascorbic acid solution were added to 10 mL of 25 mM CTAC solution. Then, 25 µL of a 0.05 M $HAuCl_4$ solution was added under vigorous stirring. The mixture was left undisturbed at room temperature for at least 30 min. *Step 2:* Once the growth was complete, another aliquot of 25 µL of a 0.05 M $HAuCl_4$ was added. After 30 min, the mixture was heat up to 75ºC during 20-30 min. *Step 3:* Finally, the gold nanoparticles suspension was cool down to 40ºC and 10 mg of NaBr and 25µL 0.05 M $HAuCl_4$ were added. The suspension was left undisturbed for 1h and finally centrifuged. The nanospheres were redispersed in 1 mL of 1 mM CTAB solution.

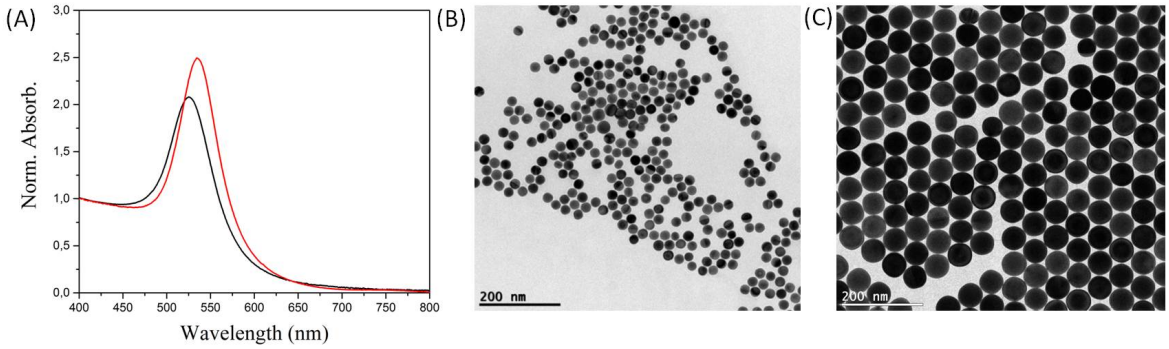

Figure S2. (A) Extinction spectra 25 nm AuNSs (black curve) and 60 nm AuNSs (red curve). Representative TEM images of synthesized 25 nm AuNSs (B) and 60 nm AuNSs (C).

UV/Vis/NIR absorption spectra of the resulting AuNRs were registered using a Cary 5000 UV-Vis-NIR (Figure S2A). All experiments were carried out at 298 K, using quartz cuvettes with optical paths of 0.1 or 1 cm. TEM images of AuNSs were obtained with a JEOL JEM-1400PLUS transmission electron microscope, operating at an acceleration voltage of 120 kV. Carbon-coated 400 square mesh copper grids were used. All samples were

centrifuged at least once before blotting on the grid. The resulting CTAB-stabilized AuNSs (CTAB-AuNSs) presented a diameter of 24 ± 2 nm and 61 ± 3 nm as determined from TEM images (Figure S2B-C).

ANTA-Cobalt AuNRs and AuNSs functionalization

Typically, 2.5 mL of 1mM PegSH aqueous solution and 2.5 mL of 100mM lipoic acid in 200 mM Hepes (pH 8) were added dropwise under stirring to 5 mL of a freshly prepared aqueous suspension of AuNRs (2 mM of Au^0, 50 μM of CTAB) and AuNSs (2 mM of Au^0, 500 μM of CTAB) consecutively. After 12 h, the excess of free PegSH and lipoic acid was removed by one centrifugation cycle (AuNRs: 6000 rpm, AuNSs: 60nm: 4000 rpm, AuNSs: 25nm: 6000 rpm 30 minutes). The precipitate was redispersed in 5 mL of 20 mM hepes solution (pH 8). Activation of the carboxylic group was performed by addition of 2.5 mL of 35 mM of EDC and 2.5 mL of 35 mM of NHS solution (20 mM hepes at pH 8). After 30 min, 5 mL of ANTA-Cobalt complex (20 mM hepes pH 8), which was previously prepared in 20 mM hepes solution by mixing 2.5 mL of 100 mM ANTA solution and 2.5 mL of 150 mM of cobalt (II) chloride solution, were added to the activate the lipoic acid functionalized AuNRs. The mixture was left undisturbed at least for 1h. After the reaction time, the AuNPs were centrifuged (25% lower rpm respect to the previous steps) for 45 min and redispersed in 15 mL of water. Two more centrifugation cycle was performed in order to obtain a final Au^0concentration of 10 mM in water.

Protein purification

Recombinant H6-RepA-WH1(A31V) and RepA-WH1(A31V) were expressed in *E. coli* and purified as previously described.[1] Protein concentration was calculated assuming a molar extinction coefficient (A_{280nm}) 11,548 $M^{-1}\cdot cm^{-1}$ per RepA-WH1(A31V) chain. UV/Vis absorption spectra of the resulting protein systems were registered using a Ultrospec 3330 (Amersham Biosciences/GE Healthcare) equipment. Protein stocks (80 μM, after concentration through Amicon PM10 filters) were kept at −70°C in 0.2 M Na_2SO_4, 15 mM Na_2HPO_4 (pH 6), 2 mM $MgSO_4$, 5 mM 2-mercaptoethanol, and 10% (v/v) glycerol.

Amyloid functionalization of AuNRs and AuNSs

Protein was dialyzed against 40 mM hepes, 100 mM Na_2SO_4 at pH 8. After dialysis, H6-RepA-WH1(A31V) and RepA-WH1(A31V) were mixed at different concentrations (2 μM to 20 μM) with gold nanoparticles (final AuNPs concentration A_{400nm}= 0.250) in a 2 ml Eppendorf tube and incubated overnight at 4°C (Figure S3,S4,S5). Then AuNPs were

centrifuged for 15 min and washed with dialysis buffer to remove excess of unbound protein. Functionalized AuNPs were resuspended again in the same buffer and stored at 4°C for further use.

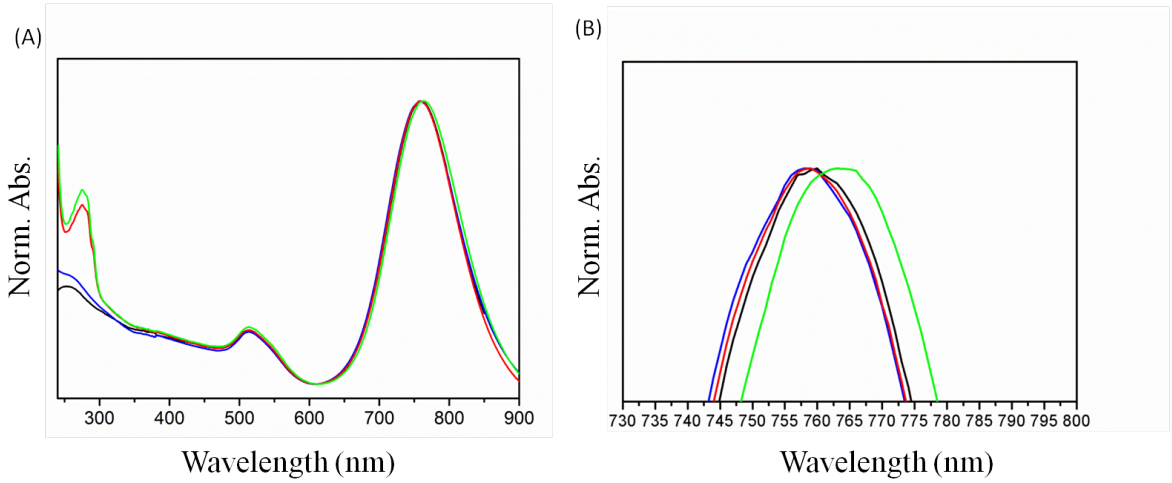

Figure S3. (A) Extinction spectra and (B) magnification of the longitudinal surface plasmon resonance of functionalized AuNRs in water **(**black curve), hepes buffer (blue curve), and after 24 h of incubation with 20 μM of RepA-WH1(A31V) (red curve) and H6-RepA-WH1(A31V) (green curve). The observed 5 nm red shift of the longitudinal LSPR in the case of H6-RepA-WH1(A31V) is ascribed to changes in the environment of the AuNRs due to protein attachment.

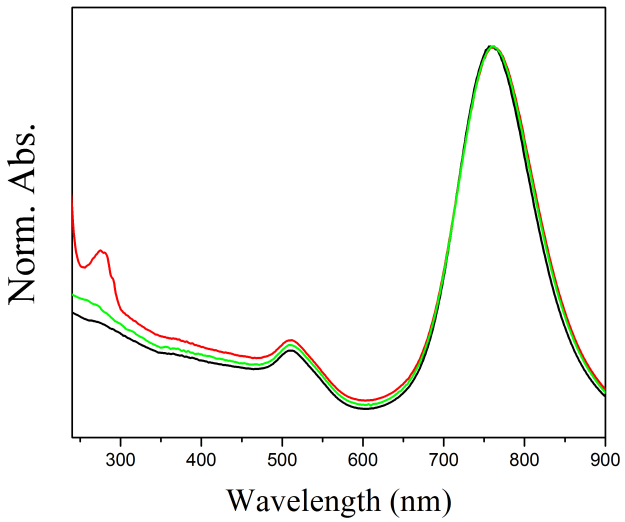

Figure S4. (A) Extinction spectra of the longitudinal surface plasmon resonance of functionalized AuNRs in buffer (black curve), incubated with H6-RepA-WH1(A31V) in 1:10^5 (red curve) and 1:50 (green curve) ratio.

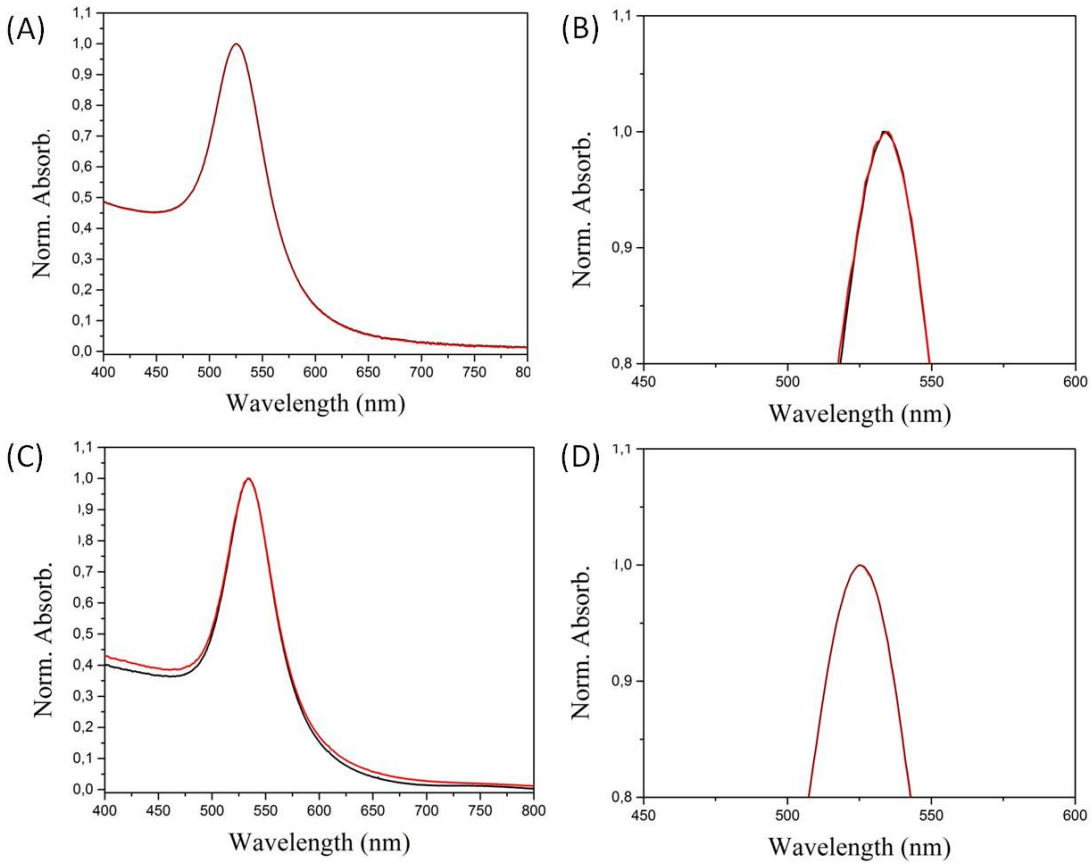

Figure S5. (A) Extinction spectra and (B) magnification of the longitudinal surface plasmon resonance of 25 nm AuNSs before (black curve) and after (red curve) incubation with 20 μM of H6-RepA-WH1(A31V). (C) Extinction spectra and (D) magnification of the longitudinal surface plasmon resonance of 60 nm AuNSs before (black curve) and after (red curve) incubation with 20 μM of H6-RepA-WH1(A31V). No red shift of the longitudinal LSPR is observed even for the bigger AuNSs.

Preparation of RepA-WH1 amyloid fibers

Fibers were assembled *in vitro*, as previously described in the literature,[1] in a final volume of 100 μL by mixing 20 μM of the purified protein RepA-WH1(A31V) in 40 mM Hepes pH 8, 0.1 M Na_2SO_4, 5 mM $MgSO_4$, 7% PEG4000, 3% MPD, and leaving the samples at 4 °C for 2–4 weeks. AuNRs functionalized with H6-RepA-WH1(A31V) were added at the beginning of the incubation at a concentration of 0.05 nM. An analogous control was conducted with non-functionalized AuNRs (Figure S6). Samples were examined by means of electron microscopy at 20 days of incubation. Briefly, samples were adsorbed on glow-discharged

400-mesh copper grids (Ted Pella), air-dried and stained with 2% uranyl acetate for 2 min. Grids were examined in a JEOL JEM-1230 transmission electron microscope, operating at 100 kV, and images were captured with a TVIPS TemCam-F416 CMOS camera.

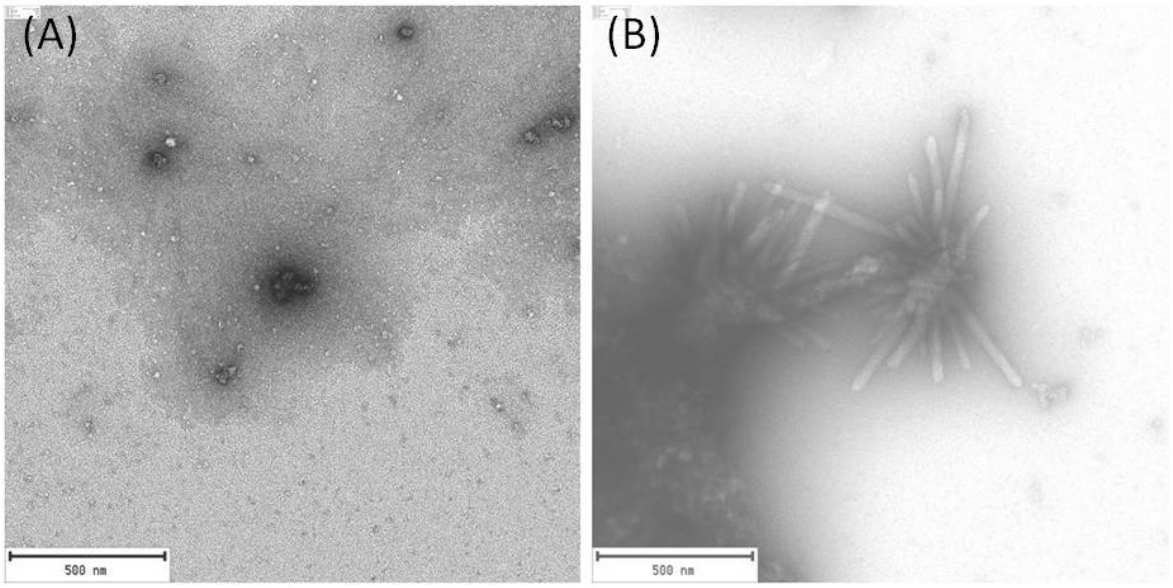

Figure S6. TEM images of amyloid fibers obtained after incubation without seeds (A) and and AuNRs without previous functionalization with H6-RepA-WH1(A31V) (B). Usage of non-functionalized AuNRs resulted in sporadic formation of fibers, meanwhile amorphous aggregation but not complete inhibition of fiber growth resulted in the absence of seeds.

Protein detection by Western/dot-blotting

RepA-WH1(A31V) was probed with the rabbit anti-WH1 primary antibody (1:3,000 in blocking solution, for 2 h at room temperature). Fifty μl of nanoparticles functionalized with H6-RepA-WH1(A31V) were diluted in 200 μl of buffer and centrifuged 15 min at 5000 rpm. The pellet was washed with 100 μl of buffer and centrifuged again for 5 min at 13000 rpm. The final pellet was resuspended in 20 μl of buffer and then analyzed by SDS-PAGE (12% polyacrylamide gel, 100 V). Protein bands in the gel were transferred to a PVDF membrane and processed as described.[2] Primary antibody (rabbit anti-WH1, 1:3000 of a 5 mg/mL antibody stock solution) was incubated for 2 h and the HRP-conjugated secondary anti-rabbit antibody (1:10.000; GE Healthcare) for 1 h. Chemiluminiscent detection was performed with the ECL prime kit (GE Healthcare) (Figure S7). All steps were performed at room temperature. Dot-blotting on serial dilutions of the soluble or AuNRs-functionalized H6-RepA-WH1(A31V) was carried out using the B3h7 anti-

amyloidogenic oligomers antibody (1:3.000) or anti-WH1 (1:5.000), and HRP-conjugated secondary antibodies (anti-mouse and rabbit, respectively, 1:5.000).[2]

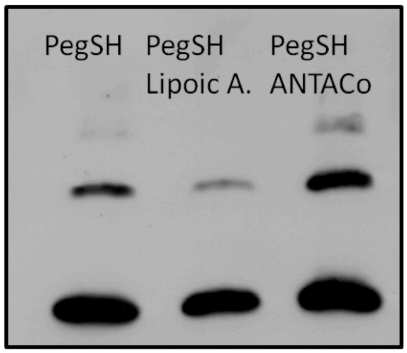

Figure S7. (A) SDS-PAGE plus Western-blotting (anti-WH1) of 20 μM H6-RepA-WH1(A31V) incubated with AuNRs functionalized only with PegSH, cofunctionalized with PegSH/lipoic acid, and with PegSH/ANTACo complex.

Immuno-electron microscopy (iEM)

Samples were adsorbed on copper grids (see above) and washed two times with bi-distilled water. Grids were floated on drops containing blocking solution (2% BSA, 0.05 % Tween-20 in PBS 1X) for 30 min. The grids were incubated with the anti-WH1 primary antibody (1:1,000) for 3 h at room temperature (see above). Samples were washed three times (10 min each) with 0.05 % Tween-20 in PBS, and then incubated 1 h with gold-conjugated (10 nm ø particles) anti-rabbit secondary antibodies (Sigma; 1:50 in blocking solution). Finally, they were washed three times with 0.05% Tween-20 in PBS and three times with bi-distilled water. Grids were then air-dried, stained with uranyl acetate and examined at the electron microscope as indicated above (Figure S8).

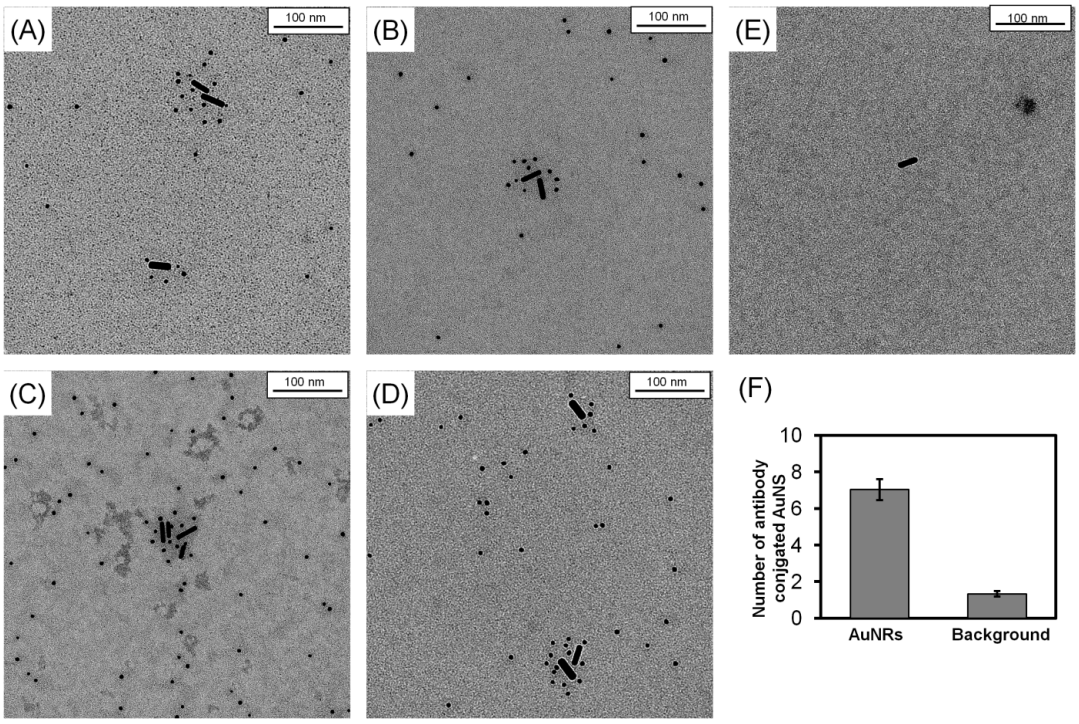

Fig S8. iEM of AuNR functionalized with H6-RepA-WH1(A31V) and incubated with the primary antibody (anti-WH1). The Au-conjugated secondary antibody (dots) cluster around the functionalized AuNRs. Several images are showed in (A), (B), (C) and (D). (E) iEM of a control experiment using naked AuNR without functionalization. (F) Quantification of the number of dots (secondary Au-conjugated antibody) around the functionalized AuNRs.

Surface Enhanced Raman Spectroscopy (SERS) characterization

SERS experiments were performed with a confocal Raman microscope (Renishaw InVia) equipped with a motorized scan stage and two Peltier-cooled CCD detectors. All SERS spectra (Table 1) were recorded on substrate and averaged over 15 single spectra measured at different points on the substrate, obtained using 785 nm laser as excitation source with fluence of 13.88 mJ/cm^2 and focusing onto the solid sample surface under ambient air conditions through a 100× objective with a numerical aperture. Effective irradiation powers were measured by a photodiode power sensor (PD300-3W, Ophir). All sample were prepared by drying a 3 µL drop of freshly prepared mixture 60 nm citrate capped gold nanoparticle solution (10 mM of Au^0)[3] (Figure S9) (previously centrifuged to removed the excess of citrate) and the AuNR-protein suspension of 1:1 ratio onto a quartz substrate (20 mM NaH_2PO_4 with 0.1 M Na_2SO_4 was used instead of hepes buffer to avoid SERS interferences from the hepes molecules).

Table 1. Band assignments for SERS spectra of native H6-WH1(A31V), low (LMWO) and high molecular weight oligomers (HMWO) of H6-WH1(A31V).[4-9]

Peak Position (cm^{-1})			Assignment	Proposed Residue
Native Conformation	*LMWO*	*HMWO*		
	720	720	Def (COO^-) / V(CS) $–H_2C–$ S Met.	
741	739	740	V(S-CH_3)	Met
759			C–C str.	
	823		C–C str. /asym. C–S–C str.	
833		831	C–C str.	
	887	890	C–C str.	
926	920	919	C–COO^- str.	Backbone
957			C–C str.	
1001	995	997	Sym. ring C-C str.	Phe
	1047		C–N str	
	1118		NH_2 rock	
1130	1130	1130	Asym. Vibr. (C-CN)/ NH_3 def.	
	1220			
1222		1222		
	1242	1242	Amide III	β-strand
1265			Amide III	α-helix
	1290	1290	Amide III	α-helix
1313			CH_2 wag	Glu Gln
	1320		CH_2 wag	Gly
1336			CH_2 wag	Tyr
	1357	1357	CH def	
1368			CH def.	
	1399	1399	COO^- sym. stretch	Backbone
1433		1433	CH2 sciss.	Glu/ Gln
	1444		CH2 sciss.	Gly/leu
1545	1545	1545	Indole vibr.	Tyr/trp
1580	1580	1580	COO^- asym. stretch.	Backbone
		1606	Sym. ring CC stretch.	Phe, Tyr
	1648	1648	Amide I	α-helix
	1670	1670	Amide I	β-sheet

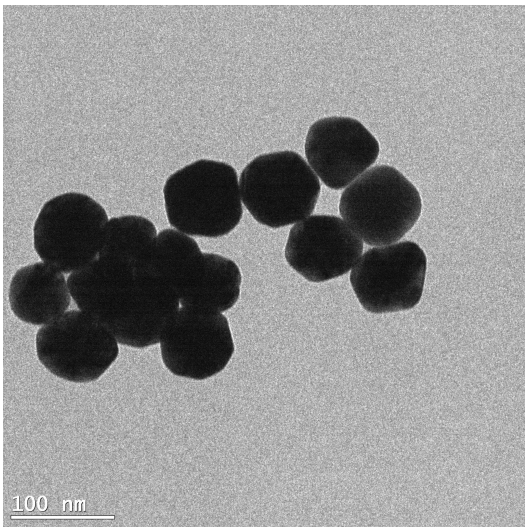

Figure S9. TEM images of citrate capped gold nanoparticles used for SERS measurements.

References

[1] Giraldo, R. *Proc. Natl. Acad. Sci. USA* **2007**, *104*, 17388–17393.
[2] Moreno-del Álamo, M.; Moreno-Díaz de la Espina, S.; Fernández-Tresguerres, M. E.; Giraldo, R. *Sci. Rep*. **2015**, *5*, 14669.
[3] Bastus, N. G.; Comenge, J.; Puntes, V. *Langmuir* **2011**, *27*, 11098-11105.
[4] Takashi Miura, G. J. T. J. in *Proteins: Structure, Function, and Engineering* (ed. : Biswas, B.B., Roy, S.) 55–99 (1995).
[5] Nemecek, D.; Stepanek, J.; Thomas, G. J. in *UNIT 17.8 Raman Spectroscopy of Proteins and Nucleoproteins, Curr. Protoc. Protein Sci.* (2013).
[6] Podstawka, E.; Ozaki, Y.; Proniewicz, L. M. *Appl Spectrosc.* **2004**, *58*, 570-580.
[7] Podstawka, E.; Ozaki, Y.; Proniewicz, L. M. *Appl Spectrosc.* **2004**, *58*, 581-90.
[8] Podstawka, E.; Ozaki, Y.; Proniewicz, L. M. *Appl Spectrosc*. **2005**, *59*, 1516-1521.
[9] Rygula, a.; Majzner, K.; Marzec, K. M.; Kaczor, A.; Pilarczyk, M.; Baranska, M. *J. Raman Spectrosc*. **2013**, *44*, 1061-1076.